Published in final edited form as:

FASEB J. 2021 March ; 35(3): e21263. doi:10.1096/fj.202001998R.

Fluid shear stress generates a unique signaling response by activating multiple TGFβ family type I receptors in osteocytes

David A. Monteiro[a,b], **Neha S. Dole**[a], **J. Luke Campos**[a], **Serra Kaya**[a], **Charles A. Schurman**[a,b], **Cassandra D. Belair**[c,d], **Tamara Alliston**[a,b,c,1]

[a]Department of Orthopaedic Surgery, University of California, San Francisco, CA, 94143, USA

[b]UC Berkeley-UCSF Graduate Program in Bioengineering, San Francisco, CA, 94143, USA

[c]The Eli and Edythe Broad Center of Regeneration Medicine and Stem Cell Research, University of California, San Francisco, CA 94143, USA

[d]Department of Urology, University of California, San Francisco, CA, 94143, USA

Abstract

Bone is a dynamic tissue that constantly adapts to changing mechanical demands. The transforming growth factor beta (TGFβ) signaling pathway plays several important roles in maintaining skeletal homeostasis by both coupling the bone-forming and bone-resorbing activities of osteoblasts and osteoclasts and by playing a causal role in the anabolic response of bone to applied loads. However, the extent to which the TGFβ signaling pathway in osteocytes is directly regulated by fluid shear stress (FSS) is unknown, despite work suggesting that fluid flow along canaliculi is a dominant physical cue sensed by osteocytes following bone compression. To investigate the effects of FSS on TGFβ signaling in osteocytes, we stimulated osteocytic OCY454 cells cultured within a microfluidic platform with FSS. We find that FSS rapidly upregulates Smad2/3 phosphorylation and TGFβ target gene expression, even in the absence of added TGFβ. Indeed, relative to treatment with TGFβ, FSS induced a larger increase in levels of pSmad2/3 and *Serpine1* that persisted even in the presence of a TGFβ receptor type I inhibitor. Our results show that FSS stimulation rapidly induces phosphorylation of multiple TGFβ family R-Smads by stimulating multimerization and concurrently activating several TGFβ and BMP type I receptors, in a manner that requires the activity of the corresponding ligand. While the individual roles of the TGFβ and BMP signaling pathways in bone mechanotransduction remain unclear, these results implicate that FSS activates both pathways to generate a downstream response that differs from that achieved by either ligand alone.

[1]**Corresponding Author:** Tamara Alliston, University of California, San Francisco, 513 Parnassus Avenue, S-1155, San Francisco, CA 94143-0514, tamara.alliston@ucsf.edu, 415-502-6523.

Author Contributions

Conceptualization, DA Monteiro, NS Dole, T Alliston; Investigation, DA Monteiro, NS Dole, JL Campos, CD Belair; Analysis, all authors; Writing – original draft, DA Monteiro; Writing – review and editing, all authors; Project Leadership, DA Monteiro, T Alliston.

Conflict of Interest statement

The authors declare no conflict of interest in connection with this article.

Keywords

osteocytes; TGFbeta; mechanobiology; microfluidics

Introduction

Cells experience concurrent biochemical and physical cues that coordinate cellular behavior through regulation of critical signaling pathways. These physical cues – substrate stiffness or topography, compression, stretch, or fluid shear stress, among others – can be transduced by cell surface mechanosensors to influence cellular decisions such as migration or differentiation [1,2]. Physical cues act in part by modulating the level or quality of biochemical signaling pathways, including the famously "context-dependent" transforming growth factor beta (TGFβ) pathway. Three different TGFβ ligands activate this pathway by binding to a pair of TGFβ type II receptors (TβRII), which then recruits a pair of TGFβ type I receptors (also called ALKs) [3]. This heterotetrameric complex then phosphorylates several downstream effectors, including the canonical TGFβ effectors Smad2 and Smad3 [4,5]. Other TGFβ family ligands, such as BMPs and activins, signal through their corresponding receptors and effectors. The specific mechanisms by which distinct biochemical and physical cues target the TGFβ pathway to determine its intensity, downstream targets, or duration remain to be fully elucidated. This is in part because these stimuli can exert multi-level control of the TGFβ signaling pathway, for example, by regulating ligand synthesis and activation; receptor trafficking and multimerization; and Smad phosphorylation and nuclear translocation [6].

Skeletal cell types utilize several of these mechanisms to calibrate the activity of the TGFβ signaling pathway based on the physical features of the extracellular matrix (ECM). To adapt to ECM stiffness or topography, cells generate cytoskeletal tension, which is required for maximal activation of Smad1 by BMPs in human mesenchymal stem cells (hMSCs) [7]. At an optimum level of cytoskeletal tension, chondrocytes exhibit increased Smad2/3 phosphorylation, a potent synergistic response to exogenous TGFβ, and maximal induction of chondrocyte gene expression [8]. Further investigation into the mechanoregulation of TGFβ signaling in chondrocytes implicated a focal adhesion-localized subpopulation of TGFβ receptors, whose spatial organization was sensitive to changes in cytoskeletal tension [9]. More specifically, subpopulations of type I and type II receptors were segregated from each other in cells with high cytoskeletal tension. Disruption of tension enabled receptor colocalization and heteromerization, suggesting a mechanism through which changes in a cell's internal mechanical environment can enhance or suppress TGFβ signaling.

Likewise, fluid shear stress (FSS) has been shown to interact with TGFβ family signaling pathways in several biological contexts [10–15], though its effects on skeletal cells remain to be explored. For example, in proximal tubular epithelial cells, exposure to FSS significantly upregulated Smad2/3 phosphorylation and nuclear translocation and transcription of TGFβ target genes [16]. Nonetheless, the mechanisms by which FSS modulates TGFβ family signaling appear to differ from one cell type to the next. Kunnen et al. report that FSS-mediated activation of TGFβ signaling is blocked in cells treated with the ALK4/5/7

inhibitor LY-364947, but also observed mild decreases of active and total TGFβ1 levels in flow media following application of FSS [16]. On the other hand, Kouzbari et al. and Albro et al. showed that levels of active TGFβ1 in platelet releasates and synovial fluid, respectively, increase after stimulation with FSS [17,18]. As a result, the extent to which this mechanism depends primarily on ligand-level, receptor-level, or downstream regulation in a cell type-specific manner remains unclear.

In bone, mechanoregulation of the TGFβ signaling pathway in response to compression is required for bone anabolism, in part because of its role in coordinating the mechanoregulation of sclerostin expression [19]. Indeed, mice expressing a dominant negative TGFβ receptor type II under control of the osteocalcin promoter exhibit minimal changes in cortical bone thickness and mineral apposition rate following a hindlimb loading regimen relative to wildtype controls. Mechanical compression of bone tissue is known to induce fluid flow within the perilacunar/canalicular network that leads to changes in fluid shear stress and hydrostatic pressure sensed by osteocytes [20,21]. However, the extent to which FSS directly regulates TGFβ signaling in these cells remains unknown. A deeper understanding of how and when FSS stimulation affects the TGFβ pathway in osteocytes is essential because careful regulation of TGFβ signaling is necessary for bone homeostasis and dysregulation can drive disease progression [22,23].

While others have evaluated the effects of FSS on cellular function and cytokine expression using osteocyte-like MLO-Y4 cells, these efforts have focused mainly on FSS inhibition of *DKK1* and *Sost* expression, induction of Wnt/β-catenin signaling, and activation of HIF-1α and AMPK inflammatory pathways, with no analysis of its role in regulating TGFβ/Smad signaling [24–26]. Likewise, in the more recently developed osteocyte-like cell line, OCY454, stimulation of fully differentiated cells with FSS significantly lowered extracellular sclerostin levels and *Sost* mRNA expression [27,28], but its link to TGFβ signaling remains to be elucidated. Thus, using a microfluidic *in vitro* platform to stimulate cells with FSS, we investigated the dynamics and effects of FSS on TGFβ signaling in OCY454 cells. Our results show that FSS rapidly enhances Smad signaling by stimulating heteromerization and activating several distinct subsets of TGFβ type I receptors, in a manner different than that which could be achieved by treatment with ligand alone.

Materials and Methods

Microfluidic device fabrication and shear stress experiments

The microfluidic devices used for shear stress experiments were fabricated using soft lithography techniques. Briefly, a 3-inch diameter silicon wafer was spin-coated with a 75 μm layer of photoresist (SU-8, Kayaku) and then exposed to UV light through a custom photomask (CAD/Art Services). After a 15-minute post-exposure bake, the unreacted photoresist was removed, followed by a 30-minute hard bake at 150°C. The chambers (Fig. 1A) had an elongated hexagonal culture area (25 mm long, 10 mm wide, 75 μm tall) with a chamber volume of ~15 μL.

Polydimethylsiloxane (PDMS, Sylgard 184, Dow) was prepared at a 10:1 elastomer/curing agent ratio, degassed for 30 minutes, poured over the silicon wafer mold, and allowed to

cure overnight at 60°C. The cured PDMS was cut from the mold (2 chambers per PDMS piece, to fit on one 25 mm x 75 mm glass slide), inlets were cored with a 1 mm biopsy punch, and the PDMS was bonded to a glass slide following exposure of mating surfaces to 40 seconds of air plasma using a plasma cleaner (PDC-32G, Harrick Plasma). PDMS chambers were sterilized with 70% ethanol and glass surfaces were coated with a rat tail collagen type I solution (CB-40236, Corning) prior to cell seeding.

For shear stress experiments, a peristaltic pump (Masterflex L/S, Masterflex) was installed within a sterile incubator and used to circulate media through microfluidic chambers to stimulate the cells precisely with the designated amounts of shear stress ($\tau = 6 \times Q \times \mu / w \times h^2$). The volumetric flow rate of the reduced-serum media (Q) was varied to achieve the desired wall shear stress (τ) experienced by the cells. The viscosity of media (μ) pumped through the chambers (with width w and height h) was estimated as that of water at 37°C. Chambers were connected to the pump with sterilized polyethylene tubing (1.19 mm ID, Scientific Commodities). Cells grown in non-flow conditions were also grown in microfluidic chambers unless otherwise indicated.

Cell culture, transfection, and reagents

OCY454 cells (gift from Paola Divieti Pajevic) are an osteocyte cell line that can undergo terminal differentiation *in vitro* [28]. Cells were grown on collagen type I-coated tissue culture treated dishes in α-MEM (12571, Gibco) supplemented with 10% fetal bovine serum and 1% Antibiotic/Antimycotic (Gibco), maintained at 33°C with 5% CO_2, and passaged every 2-3 days [28]. For plating in microfluidic devices, cells were detached with TrypLE Express (Gibco) and resuspended in media to a concentration of 4×10^6 cells/mL before seeding. After filling the microfluidic chambers with the cell suspension (~100k cells/chamber), media was replaced daily, and experiments were performed 2 days after seeding. Cells were serum starved with reduced serum media (α-MEM, 1% fetal bovine serum, 1% Antibiotic/Antimycotic) for 1 hour before treatment which was maintained during experiments.

Cells were transfected with Fugene6 (Promega) as indicated following manufacturer's guidelines. Except where noted in the figures, cells were treated as indicated with TGFβ1 (5 ng/mL), BMP4 (50 ng/mL) (both from Peprotech); 1d11 (1.25 μg/mL, Clone 1d11.16.8, BioXCell); Noggin (100 ng/mL, SRP3227, Sigma Aldrich); SB-431542 (10 μM), LDN-193189 (1 μM), LDN-214117 (1 μM), SC-79 (10 μM) (all from Selleckchem); recombinant mouse ALK1Fc (100 ng/mL, R&D Systems); and LY294002 (50 μM, Calbiochem).

Western blotting and co-immunoprecipitation

Whether grown on traditional cell culture plates or in microfluidic chambers, cells were rinsed with 4°C PBS and lysed with 4°C RIPA buffer (50 mM Tris pH 7.4, 1% NP-40, 0.25% sodium deoxycholate, 150 mM NaCl, 1 mM EDTA, supplemented with phosphatase inhibitor (A32957, Pierce), protease inhibitor (cOmplete Mini, Roche), and 1 mM PMSF). Lysates were collected by scraping plates, or by collecting RIPA eluates flowed through the chambers. Lysates were sonicated on ice using a cuphorn sonicator (5 15-second pulses, 45

seconds between pulses) and cleared by centrifugation at 10000 *g* for 10 minutes at 4°C. For western analysis, protein separation was achieved using 10% polyacrylamide gels with an SDS/PAGE protocol, prior to transfer to a nitrocellulose membrane, blocking with 5% milk, and probing with antibodies in 1% milk or 5% BSA, all of which were suspended in TBS with 0.1% Tween 20. After probing, band intensities were visualized using an Odyssey infrared imaging system (LI-COR Biosciences) and quantified using Image Studio Lite (v5.2, LI-COR Biosciences). Fold changes were normalized to beta actin, and treatment groups to unstimulated controls as indicated in the figure legends.

For co-immunoprecipitation, cell lysates were harvested as described above with ice-cold IP lysis buffer (50 mM Tris pH 7.5, 150 mM NaCl, 2 mM EDTA, 0.5% IGEPAL CA-630, 0.25% sodium deoxycholate, supplemented with protease and phosphatase inhibitors) and were incubated with Anti-FLAG M2 Magnetic Beads (Sigma Aldrich) overnight at 4°C, washed three times in TBS (5 minutes each), and eluted by boiling at 90°C (10 minutes) before western analysis.

Antibodies

Primary antibodies used in this study include: anti-phospho-Smad3 (Western blot (WB) 1:2000, rabbit, ab52903, Abcam), anti-phospho-AKT (WB 1:2000, rabbit, #4060, Cell Signaling), anti-AKT (WB 1:1000, rabbit, #9272, Cell Signaling), anti-beta actin (WB 1:2500, mouse, ab8226, Abcam), anti-Flag (WB 1:1000, mouse, F3165, Sigma Aldrich), anti-TGFβRI (proximity ligation assay, 1:200, rabbit, ab31013, Abcam), anti-TGFβRII (proximity ligation assay, 1:50, mouse, sc-17799, Santa Cruz Biotechnology), and anti-Smad2/3 (immunofluorescence 1:200, mouse, 610842, BD Biosciences). For Western blotting, anti-mouse and anti-rabbit secondary antibodies conjugated to 680 or 800 IRDye fluorophores (1:15000, LI-COR Biosciences) were used.

Quantitative RT-PCR and RNAseq

Cells were rinsed with PBS and lysed with 700 μL QIAzol (Qiagen), collected by scraping or as chamber eluate, and mRNA was purified using the miRNeasy kit (Qiagen) following manufacturer's instructions. The concentration of mRNA was determined using a NanoDrop spectrophotometer and quality for RNAseq was verified using an Agilent Bioanalyzer.

For qRT-PCR, RNA (1 μg) per sample was reverse transcribed to generate cDNA using iScript (Bio-Rad) and analysis was performed in a C1000 Thermal Cycler/CFX96 Real-Time System (Bio-Rad) using TaqMan probes (Table 1, below). 30 ng equivalent of cDNA was used for each gene, and reactions were run in duplicate, followed by quantification using the ΔΔCt method with normalization to the housekeeping gene *Rn18s* [29], which was not regulated in an FSS-dependent manner.

For RNAseq, 250 ng was used as input to library preparation using the QuantSeq 3' mRNA-Seq Library Prep Kit FWD for Illumina (Lexogen). Libraries were multiplexed and 50 bp single-end reads were generated using one lane of an Illumina HiSeq 4000 at the UCSF Center for Advanced Technology (San Francisco, CA). Sequencing adapters were trimmed using cutadapt [30] and trimmed reads were subjected to quality control analysis using FastQC (www.bioinformatics.babraham.ac.uk/projects/fastqc). Transcript expression was

quantified using the quasi-mapping-based mode of Salmon and the reference mouse genome build GRCm38—Ensembl using k-mers of length 25 with otherwise default parameters [31]. The R Statistical Computing Environment was used to obtain read counts and the DESeq2 package [32] was used to find differentially expressed genes (DEGs) with a false discovery rate (FDR) of 0.05, which were input into Enrichr for pathway analysis [33,34]. Pathways were considered significantly regulated with FDR<0.05. Our datasets are publicly available (NCBI BioProject PRJNA673223).

Imaging and image analysis

For immunofluorescence, cells were fixed with 4% paraformaldehyde in PBS (10 minutes), permeabilized with 0.5% Triton X-100 in PBS (5 minutes), and blocked with 10% goat serum in PBS (60 minutes). Cells were then incubated overnight at 4°C with primary antibody (in PBS with 2% goat serum and 3% Triton X-100). Secondary antibodies conjugated to Alexa Fluor 488 or 647 were applied for 60 minutes. For DAPI, a 300 nM solution of DAPI in PBS was applied to the cells for 5 minutes. For F-actin staining, a 1:500 solution of rhodamine phalloidin (ThermoFisher Scientific) in PBS was applied to the cells for 15 minutes. All steps were carried out at room temperature unless otherwise indicated, and three washes with PBS (5 minutes each) were carried out between all steps. Images were obtained using a DMi8 confocal laser scanning microscope (Leica) using a 40X/1.15NA oil-immersion objective.

Quantification of Smad2/3 nuclear localization was performed on individual cells using ImageJ [35] by determining the average $Smad2/3^{cyto}$ intensity value, for pixels within the cytosol, and the average $Smad2/3^{nuc}$ intensity value, for pixels within the nucleus. ΔFluorescence values ($Smad2/3^{nuc}$ - $Smad2/3^{cyto}$) were standardized to control cells (setting mean = 0 and SD = 1). The response threshold was set as one standard deviation above the mean ΔFluorescence in control cells. DAPI and rhodamine phalloidin channels were Gaussian blurred (radius=1) and used to create binary masks of nuclear and cytosolic cell regions.

For calcium imaging, cells transiently transfected with G-CaMP3 (gift from Loren Looger, Addgene plasmid #22692; RRID:Addgene_22692) [36] were grown in microfluidic chambers attached to coverslips and placed on the microscope stage before application of 0.1 Pa FSS. Images were collected from one region of interest per flow chamber. Imaging began 2-3 frames prior to FSS stimulation, and baseline G-CaMP3 fluorescence was calculated from these frames and used to normalize cellular fluorescence to account for cell-to-cell differences in intensity. Fluorescence quantification was performed using ImageJ on individual cells.

For proximity ligation assay (PLA) analysis, a Green Duolink In Situ Detection Kit (Sigma Aldrich) was used with anti-mouse MINUS and anti-rabbit PLUS probes following manufacturer's instructions. Cells were processed and treated overnight with primary antibodies following the immunofluorescence protocol above. Images were quantified using IMARIS v9.5.1 (Oxford Instruments). Raw fluorescence channels were background subtracted and puncta were identified using the Spot Detector function. Non-cell localized

puncta were removed from analysis by masking using a distance transformed, void filling surface model of actin stress fibers.

Statistical analysis

Unless otherwise indicated in the figure legends, we report mean and standard deviation (mean ± SD) from ≥3 biological replicates. Western blots shown are representative of at least 3 biological replicates. For quantification across western blots and qRT-PCR, values were normalized to unstimulated, control cells. For qRT-PCR, each sample was run in duplicate and expression was normalized to the housekeeping gene *Rn18s*. Significance was calculated with ANOVA followed by Holm-Bonferroni *post hoc* correction. In all figures $p<0.05$ was considered statistically significant.

Results

FSS rapidly induces nuclear translocation of Smad2/3 in OCY454 cells

To identify mechanisms by which fluid shear stress (FSS) regulates TGFβ signaling, we developed and validated a PDMS microfluidic culture system (Fig. 1A). The ability to precisely stimulate cells is supported by COMSOL computational modeling, which predicts laminar flow and uniform FSS conditions across the cell chamber (Fig. 1B). Accordingly, 0.1 Pa FSS activates a green fluorescent protein (GFP) Ca^{2+} reporter construct (G-CaMP3) in transfected osteocyte-like OCY454 cells. Consistent with prior reports [37], fluorescence intensity measurements revealed a synchronized increase in cytosolic Ca^{2+} levels within seconds after shear stress was applied, with no change in unstimulated control cells grown in identical conditions (Figs. 1C, 1D). Likewise, FSS rapidly activates two well-established mechanoresponsive outcomes, AKT phosphorylation (Fig. 1E) and *Ptgs2* mRNA expression (Fig. 1F).

Though FSS stimulation activates TGFβ signaling in endothelial and kidney epithelial cells [10,16], the response of TGFβ signaling to FSS in osteocytes has not yet been examined. Within 30 minutes of 0.1 Pa FSS, Smad2/3 translocates to the nucleus, just as it does in response to treatment with 5 ng/mL TGFβ (Fig. 1G). Interestingly, while stimulation with FSS and treatment with TGFβ both induce increases in nuclear-localized Smads in a majority of cells quantified, the percentage of responding cells and average difference in fluorescence were greater in TGFβ-treated cells (Fig. 1H).

TGFβ and FSS exhibit overlapping, but distinct, responses in OCY454 cells

Other studies that have evaluated FSS regulation of osteocyte-like cells have used shear stress magnitudes ranging from 0.2-0.5 Pa through 1.6-5 Pa in steady, pulsatile, and oscillatory profiles [28,38–40]. To determine the sensitivity of TGFβ signaling to these FSS parameters, levels of phosphorylated Smad2/3 were assessed after stimulating cells with 0.01, 0.1, and 1.0 Pa FSS for 30 minutes (Figs. 2A, 2B) or pulsatile and steady FSS profiles (Figs. 2C, 2D). pSmad2/3 levels were increased in all cells exposed to FSS compared to static controls even at the lowest level, with only a modest increase in pathway activation above 0.01 Pa. Likewise, no differences were observed when comparing the effects of pulsatile FSS (1 s on, 1 s off) and steady FSS. The rapid, FSS-induced phosphorylation and

nuclear translocation of these TGFβ-activated Smads suggest that FSS is sufficient to activate TGFβ signaling even in the absence of added TGFβ.

To compare the dynamics of TGFβ signaling following activation by TGFβ ligand or by FSS, we evaluated a time course of Smad2/3 phosphorylation and TGFβ-responsive gene expression in each condition. TGFβ induces Smad2/3 phosphorylation in OCY454 cells in as little as 10 minutes, with a plateau from 30-120 minutes (Figs. 2E, 2F). These dynamics matched what was observed after stimulation with 0.1 Pa FSS (Figs. 2G, 2H). In addition, both TGFβ and FSS induce the expression of the TGFβ target gene *Serpine1* within 30 minutes (Fig. 2I). Although the kinetics by which TGFβ and FSS activate TGFβ signaling outcomes are comparable, their effects differ considerably. Relative to TGFβ, FSS causes a 1.5-fold larger induction in the level of phosphorylated Smad2/3, and stimulates an approximately 10-fold greater increase in *Serpine1* mRNA levels.

Concurrent stimulation with FSS and TGFβ results in higher levels of phosphorylated Smads than either treatment alone

Since other physical cues can stimulate TGFβ signaling through mechanoactivation of latent stores of TGFβ, we tested the effect of FSS on Smad phosphorylation in the presence of saturating levels of active TGFβ. We first determined that 1 ng/mL of exogenously added active TGFβ is sufficient to maximally induce Smad phosphorylation in OCY454 cells within 30 minutes (Figs. 3A, 3B). To determine if FSS could further stimulate Smad phosphorylation, even in the presence of saturating levels of active TGFβ ligand, cells were stimulated with 0.1 Pa FSS and 5 ng/mL TGFβ. Concurrent treatment with both stimuli resulted in levels of pSmad2/3 greater than those achieved by either treatment alone. This result suggests that an FSS-dependent increase in the activation of latent TGFβ ligand alone is insufficient to explain this enhancement (Figs. 3C, 3D). Furthermore, we observed a differential effect of TGFβ and FSS on the phosphorylation of Smads. FSS preferentially induces phosphorylation of the upper band that migrates at the position of Smad2, whereas TGFβ induces phosphorylation of both Smad bands relatively equally. These qualitative and quantitative differences in Smad phosphorylation suggest that TGFβ ligand and FSS employ distinct mechanisms to activate downstream targets of TGFβ signaling in osteocytes.

FSS-mediated activation of TGFβ and BMP R-Smads require their corresponding ligand

The differential phosphorylation of Smads by FSS and TGFβ opened the possibility that Smad2 and Smad3 respond selectively to physical or biochemical cues. We also considered the possibility that the pSmad2/3 antibody cross-reacted with pSmad1/5, since FSS induces the phosphorylation of BMP-activated Smad1 and Smad5 in osteosarcoma cells [41]. The molecular weight of Smads 1 and 5 are similar to Smad2 (~52 kDa), all of which are larger than Smad3 (~49 kDa). While the pSmad2/3 antibody detected 2 bands following TGFβ treatment, it also detected the upper band in BMP4-treated OCY454 cells (Fig. 4A). Stimulation of these cells with Activin A did not result in observable changes in levels of phosphorylated Smads (data not shown). Furthermore, pSmad2/3 western analysis of Flag-immunoprecipitated lysates from OCY454 cells expressing Flag-tagged Smad1, Smad2, and Smad3 verified that the lower band is pSmad3, whereas the upper band is likely a composite of pSmad1 and pSmad2 (Fig. 4B).

Using specific ligand antagonists, we evaluated the extent to which the effects of FSS on TGFβ and BMP-responsive Smads are ligand-dependent. As expected, the TGFβ blocking antibody 1d11 significantly attenuated the TGFβ-inducible phosphorylation of both bands. However, 1d11 only partially blocked the effect of FSS (Fig. 4C). While 1d11 abrogated the FSS-inducible phosphorylation of Smad3, it had little effect on the upper band. On the other hand, treatment of cells with the BMP ligand antagonist Noggin was sufficient to selectively reduce phosphorylation of the upper molecular weight Smads induced by either BMP4 or FSS (Fig. 4D). These experiments indicate that FSS concurrently activates signaling through multiple arms of the TGFβ family signaling pathway, such that Smads canonically phosphorylated by both the TGFβ and BMP signaling pathways are activated by FSS. Furthermore, FSS activation of signaling through either Smad2/3 or Smad1 requires the corresponding TGFβ or BMP ligand.

FSS stimulation activates multiple distinct TGFβ family type I receptors in OCY454 cells

Consistent with the results in Figure 2I, FSS induces upregulation of *Serpine1* mRNA independently of added TGFβ. Like the additive effect of TGFβ and FSS on Smad phosphorylation (Figs. 3C, 3D), levels of *Serpine1* were further increased in cells that were treated concurrently with TGFβ during stimulation with FSS (Fig. 5A). To probe the role of the TGFβ type I receptor in the FSS-regulation of *Serpine1*, we pretreated cells with the ALK4/5/7 inhibitor SB-431542. SB-431542 not only attenuated the effect of FSS, but also blocked the additive contribution of TGFβ in cells treated with both stimuli concurrently, demonstrating the requirement for one or more of these receptors for the effect of FSS on *Serpine1*.

However, part of the FSS-mediated effect on *Serpine1* resists ALK4/5/7 inhibition, leading us to hypothesize that other TGFβ and BMP type I receptors also respond to FSS in osteocytes. To determine which type I receptors participate in FSS activation of Smad signaling, we stimulated cells with FSS in the presence of pharmacologic inhibitors that specifically block distinct subsets of TGFβ superfamily type I receptors [3] (Fig. 5B). While Smad phosphorylation following treatment with TGFβ was almost entirely blocked in OCY454 cells pretreated with the ALK4/5/7 inhibitor SB-431542, only a portion of the shear stress response was attenuated by that inhibitor (Fig. 5C). Indeed, the upper Smad1/2 band persisted. On the contrary, treatment with inhibitors against BMP type I receptors, specifically those against ALK1/2/3/6 (LDN-193189) or ALK1/2 (LDN-214117) had moderate effects on Smad1/2 phosphorylation induced by TGFβ but only minimal effects on its phosphorylation of Smad3. However, inhibition of these receptors completely ablated FSS-induced phosphorylation of the upper Smad1/2 band. The ALK1/2/3/6 inhibitor was the most effective antagonist of FSS-induced, but not TGFβ-induced, phosphorylation of both Smad bands, whereas the more selective ALK1/2 inhibitor allowed FSS-induced phosphorylation of the lower Smad3 band.

Because ALK1 has been implicated in chondrocyte function and chondrogenic differentiation [42], as well as in FSS-sensitive control of BMP signaling in endothelial cells [14], we further tested its role in OCY454 osteocytes using ALK1Fc, which specifically blocks signaling through ALK1 [43]. Pretreatment of these cells with recombinant murine

ALK1Fc partially blocked FSS-induced Smad phosphorylation but had little effect on Smad phosphorylation following stimulation with TGFβ or BMP4 (Fig. 5D). Collectively, these data suggest that FSS induces phosphorylation of multiple Smads by activating a combination of TGFβ and BMP type I receptors, different than that which could be achieved by treatment with either ligand alone.

RNAseq analysis supports potent FSS regulation of TGFβ superfamily signaling

To further explore the biological pathways targeted by FSS stimulation, we performed RNA sequencing analysis on unstimulated control OCY454 cells or those stimulated with 1 Pa FSS for 2 hours in the presence or absence of the ALK4/5/7 inhibitor SB-431542. To assess the similarity between biological replicates within and across samples, principal component analysis (PCA) was used to visualize relationships between groups (Fig. 6A). Interestingly, the top two principal components show that the effects of FSS (along PC1) and treatment with SB-431542 (along PC2) on OCY454 cells are mostly independent of each other.

The effect of FSS in the absence of SB-431542 yielded 1392 upregulated and 1122 downregulated differentially expressed genes (DEGs) (total = 2514 genes, FDR<0.05) (Fig. 6B). In the presence of SB-431542, stimulation with FSS yielded 1974 DEGs (1205 upregulated and 769 downregulated, Supplemental Figure S1). In-line with other studies that have evaluated changes in the osteocyte transcriptome in response to FSS [26], pathway analysis of our DEGs identified pro-inflammatory pathways such as TNFα and IL6 in addition to MAPK and TGFβ (Fig. 6C). Of the 88 genes significantly FSS-regulated genes (FDR<0.1) identified by Govey et al., 13 met the significance threshold in this study and were regulated in the same direction: *Areg*, *Bcl9l*, *Cxcl1*, *Dnajb9*, *Ell2*, *Ereg*, *Klf16*, *March9*, *Nfkbiz*, *Pik3r1*, *Ptgs2*, *Rxrb*, and *Tpp2*. Among the top 10 FSS-regulated pathways, SB-431542 inhibition of ALK4/5/7 had surprisingly modest effects on FSS regulation of the TGFβ pathway. Though the Cytoplasmic Ribosomal Proteins pathway was no longer significantly regulated by FSS in the presence of SB-431542, others were more significantly regulated, including the PluriNetWork pathway which contains genes associated with pluripotency in mice. This and other FSS-sensitive pathways include many genes implicated in TGFβ and BMP signaling (Supplemental Figure S2).

To further examine the effect of SB-431542 on FSS-inducible genes, we generated a heatmap of all DEGs from the TGFβ and PluriNetWork pathways across all samples. While no significant differences in the expression levels of many TGFβ superfamily ligands, receptors, or effectors were observed, many TGFβ and BMP target genes were upregulated by FSS, even in the presence of SB-431542, supporting the notion that FSS-regulation of TGFβ signaling occurs through TβRI-dependent and independent mechanisms (Fig. 6D). Interestingly, some of the most upregulated genes by FSS in each of these conditions were the transcription factors *Myc*, *Fos,* and *Jun*, as well as *Serpine1*. Indeed, qRT-PCR validation of established TGFβ-inducible genes revealed significant FSS-mediated increases of *Smad7*, *Cdkn1a*, *Fos*, and *Jun*, even in the presence of SB-431542 (Fig. 6E).

FSS-dependent regulation of TGFβ receptor heteromerization

Our data indicate that unlike biochemical ligands, which can activate discrete subsets of the TGFβ signaling pathways, the physical cue FSS activates a unique combination of these pathways concurrently, resulting in a pattern of gene expression that is distinct from that which could be achieved by either ligand alone. At least part of this effect results from FSS-mediated activation of multiple TGFβ and BMP type I receptors. The mechanisms involved in FSS activation of TGFβ family signaling in OCY454 cells seem to differ somewhat from those observations reported in other cell types [10–15], therefore, we evaluated mechanisms by which FSS might alter TGFβ family receptor function in osteocytes.

To examine the effect of FSS on TGFβ type I and type II receptor heteromerization, we utilized a proximity ligation assay (PLA). Relative to the negative control, in which only TβRI (ALK5) is labelled, fluorescent PLA signal identifies multimeric TβRI/TβRII complexes in baseline control conditions when both TβRI (ALK5) and TβRII are labelled (Fig. 7A). Exposure to FSS rapidly and transiently induces formation of TβRI/TβRII complexes within 10 minutes and PLA signal returns to baseline levels by 30 minutes (Fig. 7A). FSS also appears to elicit a change in puncta localization, particularly along actin stress fibers (Fig. 7A, within dashed border). Although quantitative IMARIS analysis confirmed a 2-3 fold increase in unique puncta following 10 minutes of FSS stimulation, no significant increase in the fraction of puncta in close proximity to actin fibers was observed (gold puncta, Fig. 7B; green puncta are further from actin fibers) (Fig. 7C). Further, no differences were observed in the distribution of puncta along cellular depth, thus receptor heteromerization induced by FSS stimulation does not seem to be preferentially localized to the top or bottom of the cells, but mimics the original distribution of receptor complexes (Fig. 7C).

Several established mechanisms enable precise cellular control of TGFβ receptor colocalization and heteromerization, including at specific mechanosensory sites such as the primary cilium [44] or focal adhesions [9], or through pAKT-induced shuttling of intracellular receptors to the cell membrane [45]. Among other mechanisms we explored, we perturbed AKT activity to test the hypothesis that FSS induces Smad phosphorylation by stimulating AKT-dependent membrane presentation of vesicular TGFβ receptors. Within 30 minutes of treatment, FSS but not TGFβ increased AKT phosphorylation in osteocytes (Figs. 7D, 7E). To determine the extent to which AKT activation regulates the osteocytic response to TGFβ, cells were pretreated with a PI3K/AKT inhibitor (LY294002) or agonist (SC-79) and levels of Smad phosphorylation were evaluated in the presence or absence of TGFβ (Fig. 7F). While AKT inhibition had little effect on baseline pSmad2/3 levels, it mildly enhanced the cellular response to TGFβ. On the contrary, AKT activation increased baseline Smad phosphorylation in a manner similar to FSS stimulation, and enabled an incremental increase in Smad phosphorylation upon cotreatment with TGFβ. However, FSS activation of AKT is insufficient to fully explain the effects of FSS on Smad phosphorylation, as AKT inhibition did not block FSS-mediated Smad phosphorylation (Fig. 7G). Collectively, our data show that FSS acts through a number of mechanisms, including regulated receptor multimerization and selective activation of multiple type I receptors, to induce a unique pattern of downstream signaling.

Discussion

We find that fluid shear stress activates TGFβ family signaling in a manner that differs qualitatively and quantitatively from signaling activated by either TGFβ or BMP ligands. In the osteocyte-like cell line OCY454, FSS rapidly induces Smad phosphorylation, Smad nuclear translocation, and expression of TGFβ target genes, the dynamics of which mimic that of treatment with TGFβ ligand. However, relative to TGFβ, FSS induces a larger increase in levels of pSmad2/3 and *Serpine1*. Combined stimulation with TGFβ ligand and FSS resulted in even higher levels of Smad phosphorylation and *Serpine1* gene expression than that induced by either treatment alone. The additive response to FSS and TGFβ may result from FSS-inducible TGFβ type I and type II receptor multimerization, effectively priming cells to respond to available ligand. Furthermore, FSS generates responses distinct from those achieved by either TGFβ or BMP by concurrently activating multiple TGFβ family type I receptors, providing new insight into mechanisms by which cells integrate signaling through biochemical and physical cues to generate a unique response.

In this way, discrete physical cues add diversity and specificity to the signaling outcomes produced by the molecular machinery of the TGFβ family signaling pathway. For example, the effects of TGFβ and BMP ligands are highly sensitive to the physical properties of the ECM, such that the ability of TGFβ or BMP to promote chondrogenic or osteogenic differentiation, respectively, requires an optimal level of cytoskeletal tension [7,8,46–48]. Mechanoregulation of the cellular response to TGFβ family ligands amplifies their effects at the time and site of skeletal development, but can also exacerbate pathological mineralization, such as in fibrodysplasia ossificans progressiva [49]. Among the mechanosensitive mechanisms controlling TGFβ family signaling is integrin-dependent activation of latent TGFβ ligand [50]. While FSS has been shown to activate latent TGFβ through a mechanism sensitive to FSS magnitude and flow profile (steady vs. oscillatory [17]), we find that FSS stimulates Smad phosphorylation even with saturating levels of active TGFβ ligand. This suggests that mechanoactivation of latent TGFβ is not the sole mechanism through which FSS targets this pathway in osteocytes. Further, although physical cues can also regulate mRNA levels for TGFβ ligands [51], our transcriptomic analysis revealed no significant regulation of TGFβ1 mRNA, and only a significant 1.46-fold increase in the levels of TGFβ2 mRNA along with a 2.64-fold reduction in TGFβ3 mRNA after 2 h of stimulation with 1 Pa FSS.

The TGFβ family has seven type I, five type II, and two type III receptors. Multimeric receptor complexes regulate the activity of canonical (Smad) or non-canonical (i.e. TAK1, AKT) effectors in response to diverse ligands, including TGFβs, BMPs, GDFs, activins, and inhibins [5,52]. Thus, receptor-level regulation enables cells to precisely couple activation of specific downstream effectors to distinct TGFβ family ligands. For example, the TGFβ type I receptor ALK5 responds to TGFβ by activating Smad2/3. However, in chondrocytes, ALK5 also plays an essential role in antagonizing BMP9 signaling through another type I receptor, ALK1 [53]. In osteocytes, we observe a complementary effect of ALK5 and ALK1/ALK2 activation by FSS, such that phosphorylation of both canonical TGFβ and BMP R-Smads is induced, suggesting that the effect of crosstalk between these type I receptors could depend on the cellular or mechanical context.

The mechanisms by which FSS concurrently activates multiple TGFβ receptors in osteocytes, and the physiological significance of these mechanisms in bone, remain to be determined. Nonetheless, we and others have identified mechanisms responsible for mechanoregulation of TGFβ family receptor function. Physical cues influence the heteromerization and spatial localization of TGFβ family receptors at the cell surface and within specific cellular domains. At high cytoskeletal tension, integrin-rich focal adhesions confine a population of TGFβ and BMP type I receptors (ALK5 and ALK1) and preferentially exclude TβRII. Changes in the physical microenvironment that reduce cytoskeletal tension enable colocalization and heteromerization of these type I and type II receptors and the subsequent activation of downstream Smad2/3 [9]. Chang et al. showed that αvβ3 and β1 integrins were required to observe FSS-mediated increases in Smad1/5 phosphorylation in MG63 osteosarcoma cells, but did not report their effects on TGFβ/Smad2/3 signaling [41]. A role for integrins in the FSS-mediated control of TGFβ receptor heteromerization would be exciting, especially since integrin-rich mechanosomes are thought to sense FSS in canalicular networks [54]. Indeed, we also observed a rapid, transient increase in TβRI-TβRII interactions following the onset of FSS stimulation, but technical constraints of the microfluidic chambers currently limit our ability to monitor these changes locally at focal adhesions.

In addition to integrins, FSS may exert its effects on TGFβ receptors in osteocytes through other potential mechanosensors, such as transient receptor potential subfamily V member 4 (TRPV4) ion channels and the primary cilium. FSS-induced activation of NADPH oxidase 2 (NOX2) in osteocytes generates reactive oxygen species that drive Ca^{2+} influx through TRPV4 [55]. In MLO-Y4 osteocyte-like cells, intact primary cilia were implicated in the FSS-dependent induction of *Ptgs2* mRNA [56]. Given the regulated localization of TGFβ and BMP receptors in the primary cilium and at the ciliary base [44,57,58], an attractive model posits that FSS regulates TGFβ family signaling in a cilia-dependent manner. However, studies by Kunnen et al. of FSS-inducible TGFβ family signaling in renal epithelial cells found that cilia ablation failed to block FSS-induced Smad2/3 phosphorylation or FSS-dependent EMT [16]. Likewise, we observed preservation of FSS-inducible Smad2/3 phosphorylation even upon ablation of the primary cilia in MLO-Y4 osteocyte-like cells and after ciliation in IMCD3 kidney epithelial cells (Supplemental Figure S3). We further examined the possibility that FSS-dependent activation of AKT promotes the translocation of sequestered intracellular TGFβ receptors to the cell surface where they gain access to TGFβ ligand [45,59]. Though we observed rapid AKT activation upon stimulation with FSS, AKT inhibition did not completely block FSS-induced Smad phosphorylation in the current study.

Future studies can derive mechanistic insight and clinical relevance from prior work on FSS regulation of BMP signaling in endothelial cells. FSS sensitizes endothelial cells to BMP9 signaling by stimulating association between type I (ALK1) and type III (endoglin) receptors [13]. Human loss-of-function mutations in either ALK1 or endoglin prevent the FSS-dependent control of BMP signaling in endothelial cells, resulting in arteriovenous malformations in hereditary hemorrhagic telangiectasia (HHT) [13]. ALK1 is also an attractive candidate receptor for FSS-inducible activation of Smad phosphorylation in osteocytes. ALK1 responds to both TGFβ and BMP ligands [3,42,60] and all three of the

ALK1 inhibitors tested in the current study antagonize FSS-inducible Smad phosphorylation. Though endoglin is highly expressed in endothelial cells [61], other mesenchymal lineage cell types also express endoglin and the other TGFβ family type III receptor, betaglycan [62,63]. Additional research will be needed to identify the specific receptors and mechanisms by which FSS alters the type and magnitude of TGFβ family signaling in osteocytes, as well as to examine these mechanisms in more differentiated osteocytes and *in vivo*.

The complex roles of these intersecting TGFβ family pathways in the context of the skeleton have yet to be fully understood; however, both TGFβ and BMP signaling are fundamental in skeletal development and in the anabolic response of bone to applied loads [19,64,65]. Receptor-level regulation of TGFβ family signaling appears to be essential to maintaining skeletal homeostasis. For example, mice with an osteocyte-intrinsic knockout of TβRII exhibit disrupted perilacunar/canalicular remodeling and poor bone quality [22]. Likewise, fibrodysplasia ossificans progressiva is the result of a gain-of-function mutation in the BMP type I receptor ALK2 [49]. Future studies using osteocyte-specific mutations in different TGFβ family type I, II, and III receptors could clarify the precise role of these proteins in coordinating the osteocyte response to mechanical load. In conclusion, we find that fluid shear stress rapidly and concurrently activates TGFβ and BMP signaling through distinct subsets of TGFβ family type I receptors, revealing a novel mechanism by which physical cues calibrate TGFβ family signaling.

Supplementary Material

Refer to Web version on PubMed Central for supplementary material.

Acknowledgements

The authors wish to thank Roberto Falcon-Banchs and Lydia Sohn for their expertise and assistance with microfluidic device design and validation and soft lithography capabilities and Darnell Cuylear for expert technical assistance and methods development. This work was supported by National Science Foundation grant 1636331 (TA), National Institutes of Health grants R01DE019284 and R21AR070403 (TA), and the Department of Defense through the National Defense Science and Engineering Graduate (NDSEG) Fellowship (DM).

Nonstandard Abbreviations

ALK	activin receptor-like kinase
BMP	bone morphogenetic protein
ECM	extracellular matrix
FSS	fluid shear stress
IL6	interleukin 6
MAPK	mitogen-activated protein kinase
PI3K/AKT	phosphoinositide 3-kinase / protein kinase B
PLA	proximity ligand assay

Ptgs2	prostaglandin-endoperoxide synthase 2
RIPA	radioimmunoprecipitation assay
TβRI/TβRII	transforming growth factor beta receptor I/II
TGFβ	transforming growth factor beta
TNFα	tumor necrosis factor alpha

References

1. Rape AD et al. (2015) A synthetic hydrogel for the high-throughput study of cell-ECM interactions. Nat. Commun 6, 8129 [PubMed: 26350361]
2. Guilak F et al. (2009) Control of stem cell fate by physical interactions with the extracellular matrix. Cell Stem Cell 5, 17–26 [PubMed: 19570510]
3. Heldin C-H and Moustakas A (2016) Signaling Receptors for TGF-β Family Members. Cold Spring Harb. Perspect. Biol 8,
4. Massagué J (1998) TGF-beta signal transduction. Annu. Rev. Biochem 67, 753–791 [PubMed: 9759503]
5. Feng X-H and Derynck R (2005) Specificity and versatility in tgf-beta signaling through Smads. Annu. Rev. Cell Dev. Biol 21, 659–693 [PubMed: 16212511]
6. Hinz B (2015) The extracellular matrix and transforming growth factor-beta1: Tale of a strained relationship. Matrix Biol. 47, 54–65 [PubMed: 25960420]
7. Wang Y-K et al. (2012) Bone morphogenetic protein-2-induced signaling and osteogenesis is regulated by cell shape, RhoA/ROCK, and cytoskeletal tension. Stem Cells Dev. 21, 1176–1186 [PubMed: 21967638]
8. Allen JL et al. (2012) ECM stiffness primes the TGFbeta pathway to promote chondrocyte differentiation. Mol. Biol. Cell 23, 3731–3742 [PubMed: 22833566]
9. Rys JP et al. (2015) Discrete spatial organization of TGFbeta receptors couples receptor multimerization and signaling to cellular tension. Elife 4, e09300 [PubMed: 26652004]
10. Walshe TE et al. (2013) The role of shear-induced transforming growth factor-beta signaling in the endothelium. Arterioscler. Thromb. Vasc. Biol 33, 2608–2617 [PubMed: 23968981]
11. Zhou J et al. (2012) Force-specific activation of Smad1/5 regulates vascular endothelial cell cycle progression in response to disturbed flow. Proc. Natl. Acad. Sci. U. S. A 109, 7770–7775 [PubMed: 22550179]
12. Baeyens N et al. (2015) Vascular remodeling is governed by a VEGFR3-dependent fluid shear stress set point. Elife 4,
13. Baeyens N et al. (2016) Defective fluid shear stress mechanotransduction mediates hereditary hemorrhagic telangiectasia. J. Cell Biol 214, 807–816 [PubMed: 27646277]
14. Laux DW et al. (2013) Circulating Bmp10 acts through endothelial Alk1 to mediate flow-dependent arterial quiescence. Development 140, 3403–3412 [PubMed: 23863480]
15. Utsunomiya T et al. (2016) Transforming Growth Factor-beta Signaling Cascade Induced by Mechanical Stimulation of Fluid Shear Stress in Cultured Corneal Epithelial Cells. Invest. Ophthalmol. Vis. Sci 57, 6382–6388 [PubMed: 27898984]
16. Kunnen SJ et al. (2017) Fluid shear stress-induced TGF-beta/ALK5 signaling in renal epithelial cells is modulated by MEK1/2. Cell. Mol. Life Sci 74, 2283–2298 [PubMed: 28168444]
17. Kouzbari K et al. (2019) Oscillatory shear potentiates latent TGF-beta1 activation more than steady shear as demonstrated by a novel force generator. Sci. Rep 9, 6065 [PubMed: 30988341]
18. Albro MB et al. (2012) Shearing of synovial fluid activates latent TGF-β. Osteoarthr. Cartil 20, 1374–1382
19. Nguyen J et al. (2013) Load regulates bone formation and Sclerostin expression through a TGFbeta-dependent mechanism. PLoS One 8, e53813 [PubMed: 23308287]

20. Morrell AE et al. (2018) Mechanically induced Ca(2+) oscillations in osteocytes release extracellular vesicles and enhance bone formation. Bone Res. 6, 6 [PubMed: 29581909]
21. Moore ER et al. (2018) Adenylyl cyclases and TRPV4 mediate Ca(2+)/cAMP dynamics to enhance fluid flow-induced osteogenesis in osteocytes. J. Mol. Biochem 7, 48–59 [PubMed: 31123666]
22. Dole NS et al. (2017) Osteocyte-Intrinsic TGF-beta Signaling Regulates Bone Quality through Perilacunar/Canalicular Remodeling. Cell Rep. 21, 2585–2596 [PubMed: 29186693]
23. Blaney Davidson EN et al. (2009) Increase in ALK1/ALK5 ratio as a cause for elevated MMP-13 expression in osteoarthritis in humans and mice. J. Immunol 182, 7937–7945 [PubMed: 19494318]
24. Yan Z et al. (2018) Fluid shear stress improves morphology, cytoskeleton architecture, viability, and regulates cytokine expression in a time-dependent manner in MLO-Y4 cells. Cell Biol. Int 42, 1410–1422 [PubMed: 30022568]
25. Govey PM et al. (2014) Integrative transcriptomic and proteomic analysis of osteocytic cells exposed to fluid flow reveals novel mechano-sensitive signaling pathways. J. Biomech 47, 1838–1845 [PubMed: 24720889]
26. Govey PM et al. (2015) Mapping the osteocytic cell response to fluid flow using RNA-Seq. J. Biomech 48, 4327–4332 [PubMed: 26573903]
27. Xu LH et al. (2019) OCY454 Osteocytes as an in Vitro Cell Model for Bone Remodeling Under Mechanical Loading. J. Orthop. Res. Off. Publ. Orthop. Res. Soc 37, 1681–1689
28. Spatz JM et al. (2015) The Wnt Inhibitor Sclerostin Is Up-regulated by Mechanical Unloading in Osteocytes in Vitro. J. Biol. Chem 290, 16744–16758 [PubMed: 25953900]
29. Schmittgen TD and Livak KJ (2008) Analyzing real-time PCR data by the comparative C(T) method. Nat. Protoc 3, 1101–1108 [PubMed: 18546601]
30. Martin M (2011) Cutadapt removes adapter sequences from high-throughput sequencing reads. EMBnet.journal; Vol 17, No 1 Next Gener. Seq. Data Anal. - 10.14806/ej.17.1.200 at <http://journal.embnet.org/index.php/embnetjournal/article/view/200>
31. Patro R et al. (2017) Salmon provides fast and bias-aware quantification of transcript expression. Nat. Methods 14, 417–419 [PubMed: 28263959]
32. Love MI et al. (2014) Moderated estimation of fold change and dispersion for RNA-seq data with DESeq2. Genome Biol. 15, 550 [PubMed: 25516281]
33. Chen EY et al. (2013) Enrichr: interactive and collaborative HTML5 gene list enrichment analysis tool. BMC Bioinformatics 14, 128 [PubMed: 23586463]
34. Kuleshov MV et al. (2016) Enrichr: a comprehensive gene set enrichment analysis web server 2016 update. Nucleic Acids Res. 44, W90–7 [PubMed: 27141961]
35. Schneider CA et al. (2012) NIH Image to ImageJ: 25 years of image analysis. Nat. Methods 9, 671–675 [PubMed: 22930834]
36. Tian L et al. (2009) Imaging neural activity in worms, flies and mice with improved GCaMP calcium indicators. Nat. Methods 6, 875–881 [PubMed: 19898485]
37. Jin X et al. (2014) Cilioplasm is a cellular compartment for calcium signaling in response to mechanical and chemical stimuli. Cell. Mol. Life Sci 71, 2165–2178 [PubMed: 24104765]
38. Wittkowske C et al. (2016) In Vitro Bone Cell Models: Impact of Fluid Shear Stress on Bone Formation. Front. Bioeng. Biotechnol 4, 87 [PubMed: 27896266]
39. Kamel MA et al. (2010) Activation of β-catenin signaling in MLO-Y4 osteocytic cells versus 2T3 osteoblastic cells by fluid flow shear stress and PGE2: Implications for the study of mechanosensation in bone. Bone 47, 872–881 [PubMed: 20713195]
40. Li J et al. (2012) Effect of oscillating fluid flow stimulation on osteocyte mRNA expression. J. Biomech 45, 247–251 [PubMed: 22119108]
41. Chang S-F et al. (2008) Tumor cell cycle arrest induced by shear stress: Roles of integrins and Smad. Proc. Natl. Acad. Sci. U. S. A 105, 3927–3932 [PubMed: 18310319]
42. de Kroon LMG et al. (2015) Activin Receptor-Like Kinase Receptors ALK5 and ALK1 Are Both Required for TGFβ-Induced Chondrogenic Differentiation of Human Bone Marrow-Derived Mesenchymal Stem Cells. PLoS One 10, e0146124 [PubMed: 26720610]

43. Mitchell D et al. (2010) ALK1-Fc inhibits multiple mediators of angiogenesis and suppresses tumor growth. Mol. Cancer Ther 9, 379–388 [PubMed: 20124460]
44. Labour M-N et al. (2016) TGFbeta1 - induced recruitment of human bone mesenchymal stem cells is mediated by the primary cilium in a SMAD3-dependent manner. Sci. Rep 6, 35542 [PubMed: 27748449]
45. Budi EH et al. (2019) Integration of TGF-β-induced Smad signaling in the insulin-induced transcriptional response in endothelial cells. Sci. Rep 9, 16992 [PubMed: 31740700]
46. McBeath R et al. (2004) Cell shape, cytoskeletal tension, and RhoA regulate stem cell lineage commitment. Dev. Cell 6, 483–495 [PubMed: 15068789]
47. Park JS et al. (2011) The effect of matrix stiffness on the differentiation of mesenchymal stem cells in response to TGF-β. Biomaterials 32, 3921–3930 [PubMed: 21397942]
48. Kwon S-H et al. (2013) Modulation of BMP-2-induced chondrogenic versus osteogenic differentiation of human mesenchymal stem cells by cell-specific extracellular matrices. Tissue Eng. Part A 19, 49–58 [PubMed: 23088504]
49. Stanley A et al. (2019) Elevated BMP and Mechanical Signaling Through YAP1/RhoA Poises FOP Mesenchymal Progenitors for Osteogenesis. J. bone Miner. Res. Off. J. Am. Soc. Bone Miner. Res 34, 1894–1909
50. Klingberg F et al. (2014) Prestress in the extracellular matrix sensitizes latent TGF-beta1 for activation. J. Cell Biol 207, 283–297 [PubMed: 25332161]
51. Rys JP et al. (2016) Mechanobiology of TGFbeta signaling in the skeleton. Matrix Biol. 52–54, 413–425
52. Derynck R and Zhang YE (2003) Smad-dependent and Smad-independent pathways in TGF-beta family signalling. Nature 425, 577–584 [PubMed: 14534577]
53. Wang W et al. (2019) The TGFβ type I receptor TGFβRI functions as an inhibitor of BMP signaling in cartilage. Proc. Natl. Acad. Sci. U. S. A 116, 15570–15579 [PubMed: 31311865]
54. Cabahug-Zuckerman P et al. (2018) Potential role for a specialized β(3) integrin-based structure on osteocyte processes in bone mechanosensation. J. Orthop. Res. Off. Publ. Orthop. Res. Soc 36, 642–652
55. Lyons JS et al. (2017) Microtubules tune mechanotransduction through NOX2 and TRPV4 to decrease sclerostin abundance in osteocytes. Sci. Signal 10,
56. Malone AMD et al. (2007) Primary cilia mediate mechanosensing in bone cells by a calcium-independent mechanism. Proc. Natl. Acad. Sci. U. S. A 104, 13325–13330 [PubMed: 17673554]
57. Clement CA et al. (2013) TGF-beta signaling is associated with endocytosis at the pocket region of the primary cilium. Cell Rep. 3, 1806–1814 [PubMed: 23746451]
58. Xie Y-F et al. (2016) Pulsed electromagnetic fields stimulate osteogenic differentiation and maturation of osteoblasts by upregulating the expression of BMPRII localized at the base of primary cilium. Bone 93, 22–32 [PubMed: 27622883]
59. Duan D and Derynck R (2019) Transforming growth factor-beta (TGF-beta)-induced up-regulation of TGF-beta receptors at the cell surface amplifies the TGF-beta response. J. Biol. Chem 294, 8490–8504 [PubMed: 30948511]
60. Goumans MJ et al. (2003) Activin receptor-like kinase (ALK)1 is an antagonistic mediator of lateral TGFbeta/ALK5 signaling. Mol. Cell 12, 817–828 [PubMed: 14580334]
61. Lebrin F et al. (2004) Endoglin promotes endothelial cell proliferation and TGF-beta/ALK1 signal transduction. EMBO J. 23, 4018–4028 [PubMed: 15385967]
62. Finnson KW et al. (2010) Endoglin differentially regulates TGF-β-induced Smad2/3 and Smad1/5 signalling and its expression correlates with extracellular matrix production and cellular differentiation state in human chondrocytes. Osteoarthr. Cartil 18, 1518–1527
63. Cook LM et al. (2019) Betaglycan drives the mesenchymal stromal cell osteogenic program and prostate cancer-induced osteogenesis. Oncogene 38, 6959–6969 [PubMed: 31409900]
64. Wu M et al. (2016) TGF-β and BMP signaling in osteoblast, skeletal development, and bone formation, homeostasis and disease. Bone Res. 4, 16009 [PubMed: 27563484]
65. Nguyen J et al. (2020) CYLD, a mechanosensitive deubiquitinase, regulates TGFβ signaling in load-induced bone formation. Bone 131, 115148 [PubMed: 31715338]

66. Shannon P et al. (2003) Cytoscape: a software environment for integrated models of biomolecular interaction networks. Genome Res. 13, 2498–2504 [PubMed: 14597658]

67. Kutmon M et al. (2014) WikiPathways App for Cytoscape: Making biological pathways amenable to network analysis and visualization. F1000Research 3, 152 [PubMed: 25254103]

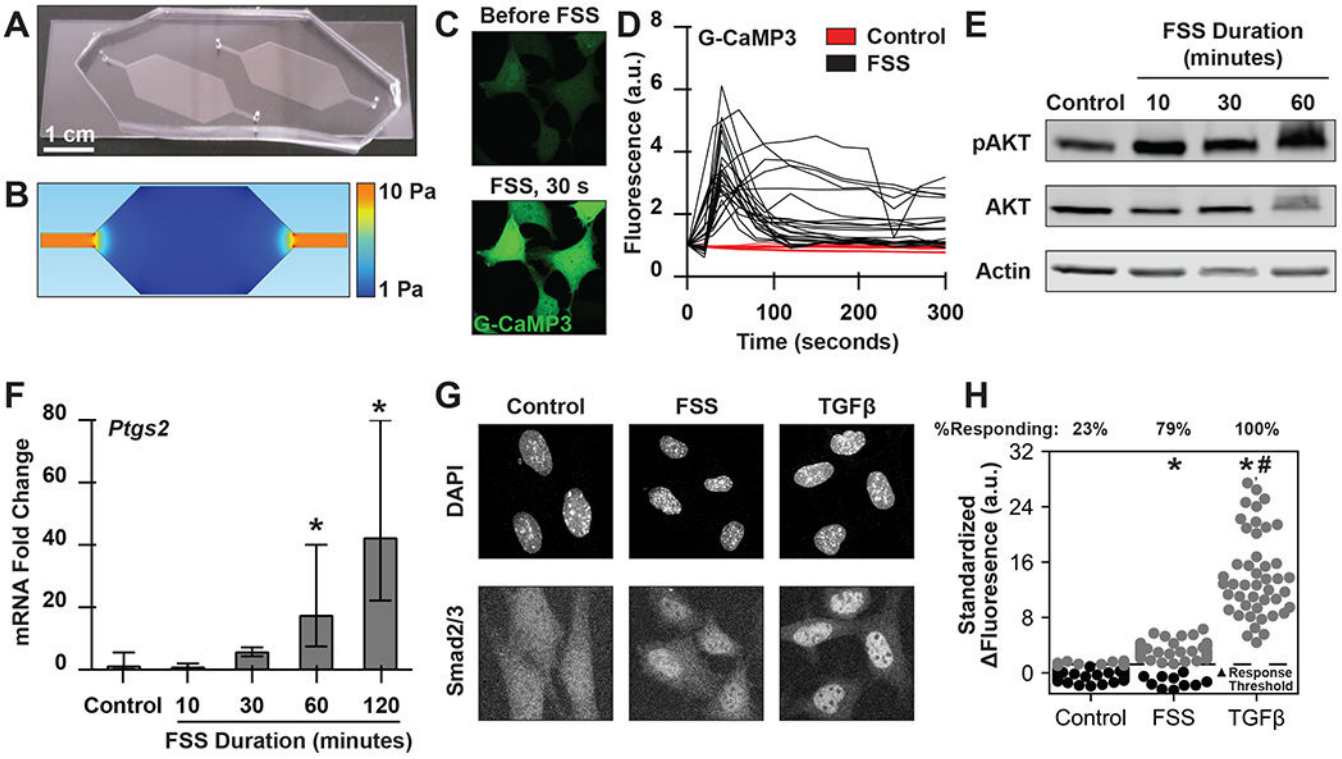

Figure 1: FSS rapidly induces nuclear translocation of Smad2/3 in OCY454 cells.

(A, B) Fluid flow through the elongated hexagonal polydimethylsiloxane (PDMS) microfluidic chambers designed and used in FSS experiments was modeled using COMSOL. (C, D) Images and fluorescence intensity quantification of individual OCY454 cells transfected with the calcium reporter G-CaMP3 prior to and following stimulation with 0.1 Pa FSS, normalized to initial cellular intensity (n=3-6 biological replicates). (E) Western analysis of AKT phosphorylation following stimulation with 0.1 Pa FSS. (F) qRT-PCR analysis of mechanoresponsive gene *Ptgs2* following stimulation with 1 Pa FSS, normalized to control cells. (G) Representative images of Smad2/3 nuclear localization in control cells or following 30-minute treatments with FSS (0.1 Pa) or TGFβ (5 ng/mL). (H) Fluorescence quantification on individual OCY454 cells showing differences in (nuclear – cytosolic) Smad2/3 intensity and %responding cells per condition (standardized to controls, n=3 biological replicates). *p<0.05 compared to unstimulated cells and #p<0.05 compared to FSS-stimulated cells.

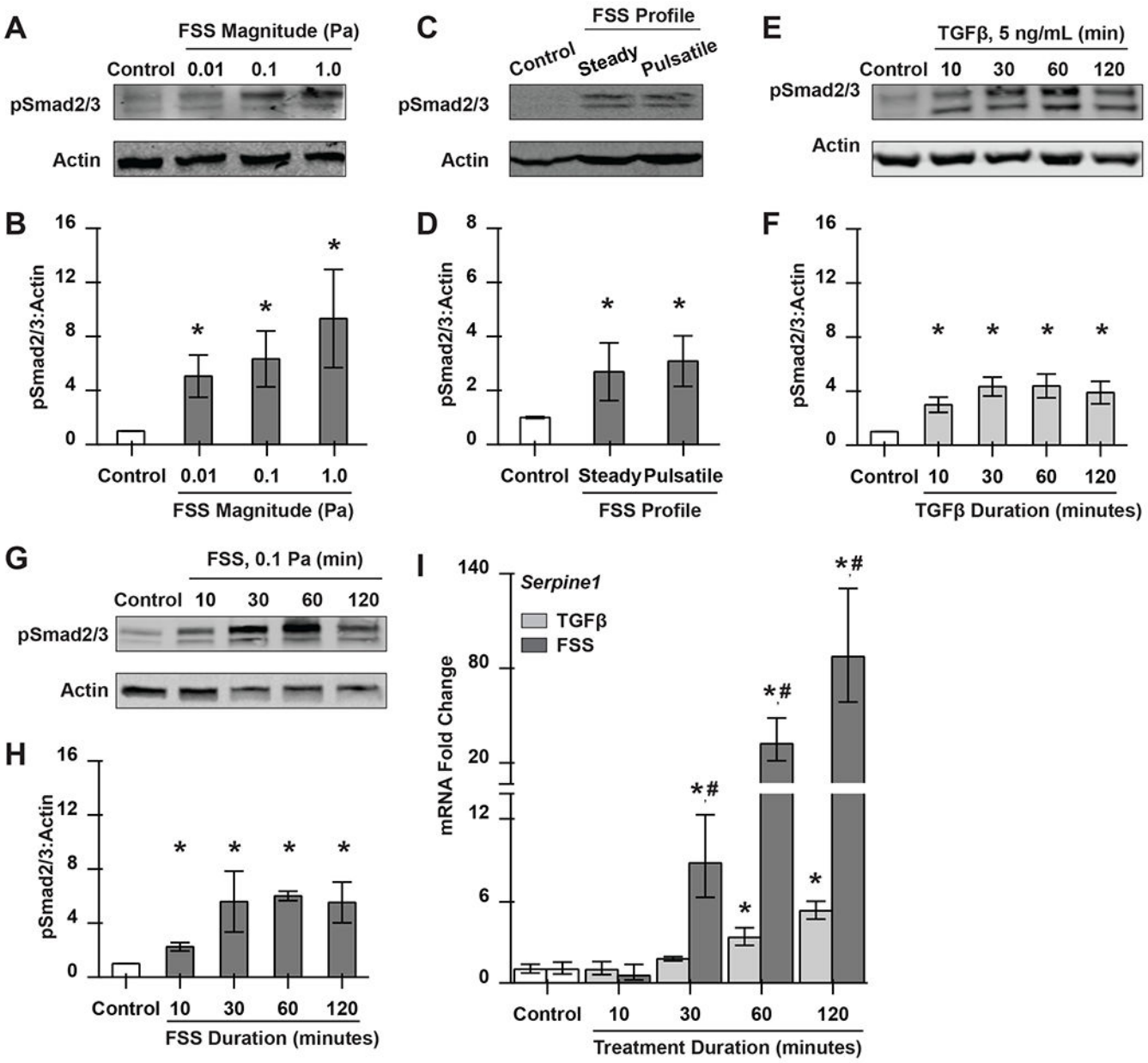

Figure 2: TGFβ and FSS exhibit overlapping, but distinct, responses in OCY454 cells.

(A – H) Western analysis and quantification of Smad phosphorylation in OCY454 cells grown in control conditions or following stimulation with steady or pulsatile (1 s on, 1 s off) FSS for 30 minutes as labeled (A - D), or a time-course of TGFβ treatment (E, F) or FSS stimulation (G, H). FSS profile is steady unless otherwise indicated. (I) qRT-PCR analysis of TGFβ pathway target gene *Serpine1* in control, TGFβ-treated, or FSS-stimulated cells. All values normalized to control cells. *p<0.05 compared to unstimulated cells and #p<0.05 compared to TGFβ-treated cells.

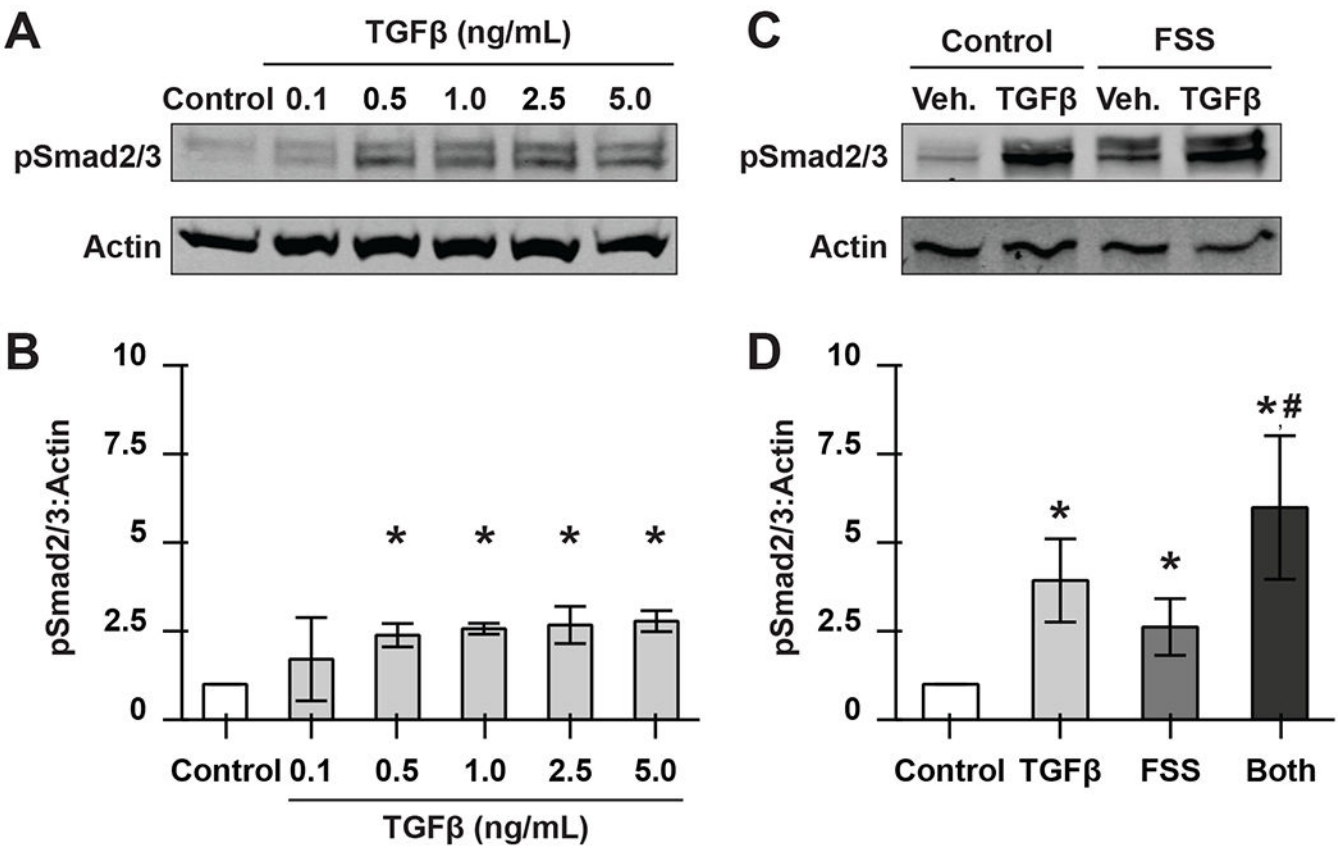

Figure 3: Concurrent stimulation with FSS and TGFβ results in higher levels of phosphorylated Smads than either treatment alone.

(A, B) Western analysis and quantification of control or TGFβ-treated OCY454 cells grown in cell culture dishes for 30 minutes, normalized to control cells. (C, D) Western analysis and quantification of OCY454 cells grown in microfluidic devices in the absence of stimulation or following 30-minute treatment with TGFβ (5 ng/mL) and/or FSS (0.1 Pa). All values normalized to control cells. *$p<0.05$ compared to unstimulated cells and #$p<0.05$ compared to FSS-stimulated group.

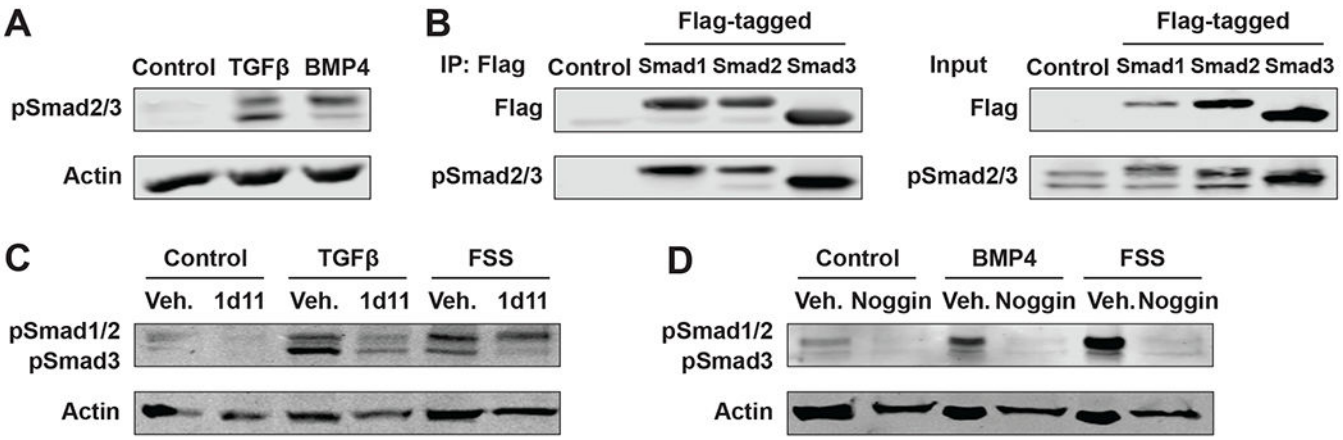

Figure 4: FSS-mediated activation of TGFβ and BMP R-Smads require their corresponding ligand.

(A) Representative western analysis of control or ligand-treated cells grown in culture dishes revealing independent regulation of pSmad bands. (B) Anti-Flag co-immunoprecipitation (left panels) or western (Input, right panels) of lysates from control or Flag-Smad transfected OCY454 cells, followed by corresponding western analysis with antibodies against Flag or pSmad2/3. (C, D) Representative western analysis of cells pretreated (60 minutes) with vehicle, 1d11 TGFβ-blocking antibody (C), or the BMP ligand antagonist Noggin (D) followed by stimulation (30 minutes) with TGFβ (5 ng/mL), BMP4 (50 ng/mL), or FSS (0.1 Pa) with Smads labeled as identified in B.

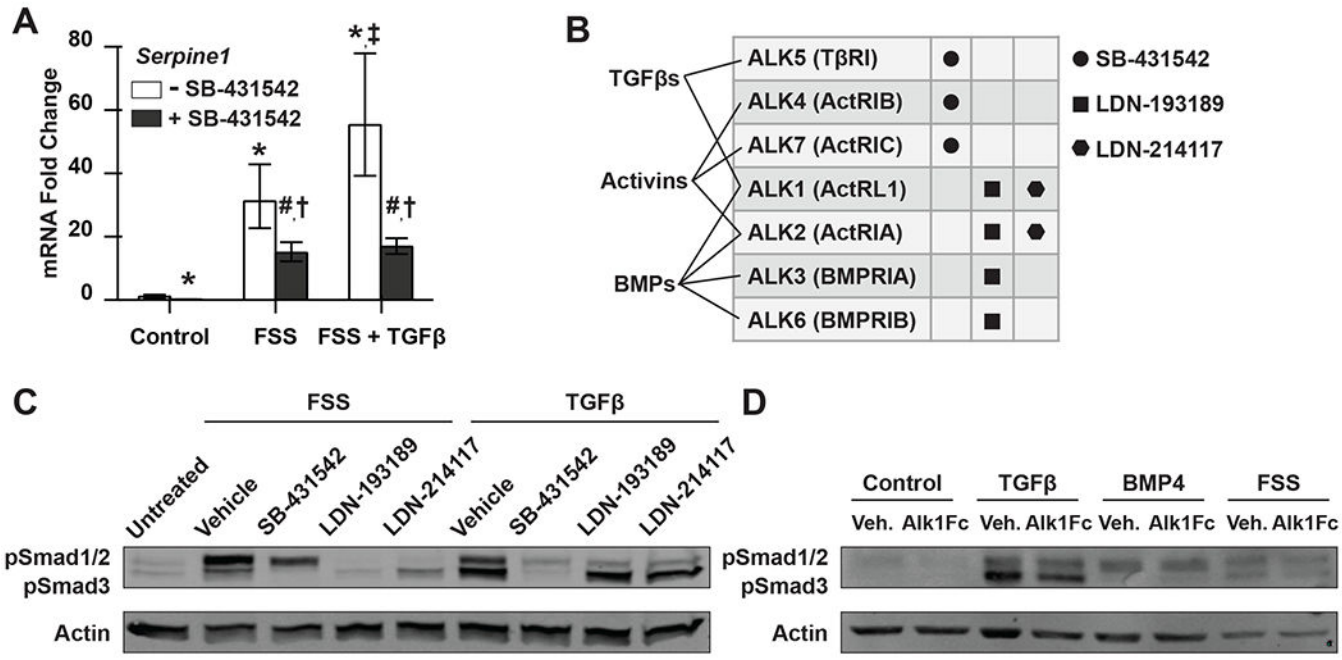

Figure 5: FSS stimulation activates multiple distinct TGFβ family type I receptors in OCY454 cells.

(A) qRT-PCR analysis of TGFβ target gene *Serpine1* after 60-minute treatment with vehicle or SB-431542 followed by 120-minute treatment with TGFβ or FSS stimulation as indicated (n=4 biological replicates). All values normalized to control cells. *p<0.05 compared to unstimulated cells and #p<0.05 compared to SB-treated controls; †p<0.05 compared to corresponding treatment group without SB-431542, ‡p<0.05 compared to FSS-stimulated cells. (B, C) Representative western analysis of Smad phosphorylation in control cells and cells pretreated (60 minutes) with vehicle or an inhibitor of a subset of TGFβ type I receptors (SB-431542, ALK4/5/7 inhibitor; LDN-193189, ALK1/2/3/6 inhibitor; LDN-214117, ALK1/2 inhibitor, as shown in B), followed by treatment (30 minutes) with TGFβ or FSS (C) (n=3 biological replicates). (D) Representative western analysis of cells pretreated (60 minutes) with ALK1Fc followed by treatment (30 minutes) with TGFβ, BMP4, or FSS (n=2 biological replicates, non-flow conditions were collected from cells grown in well plates).

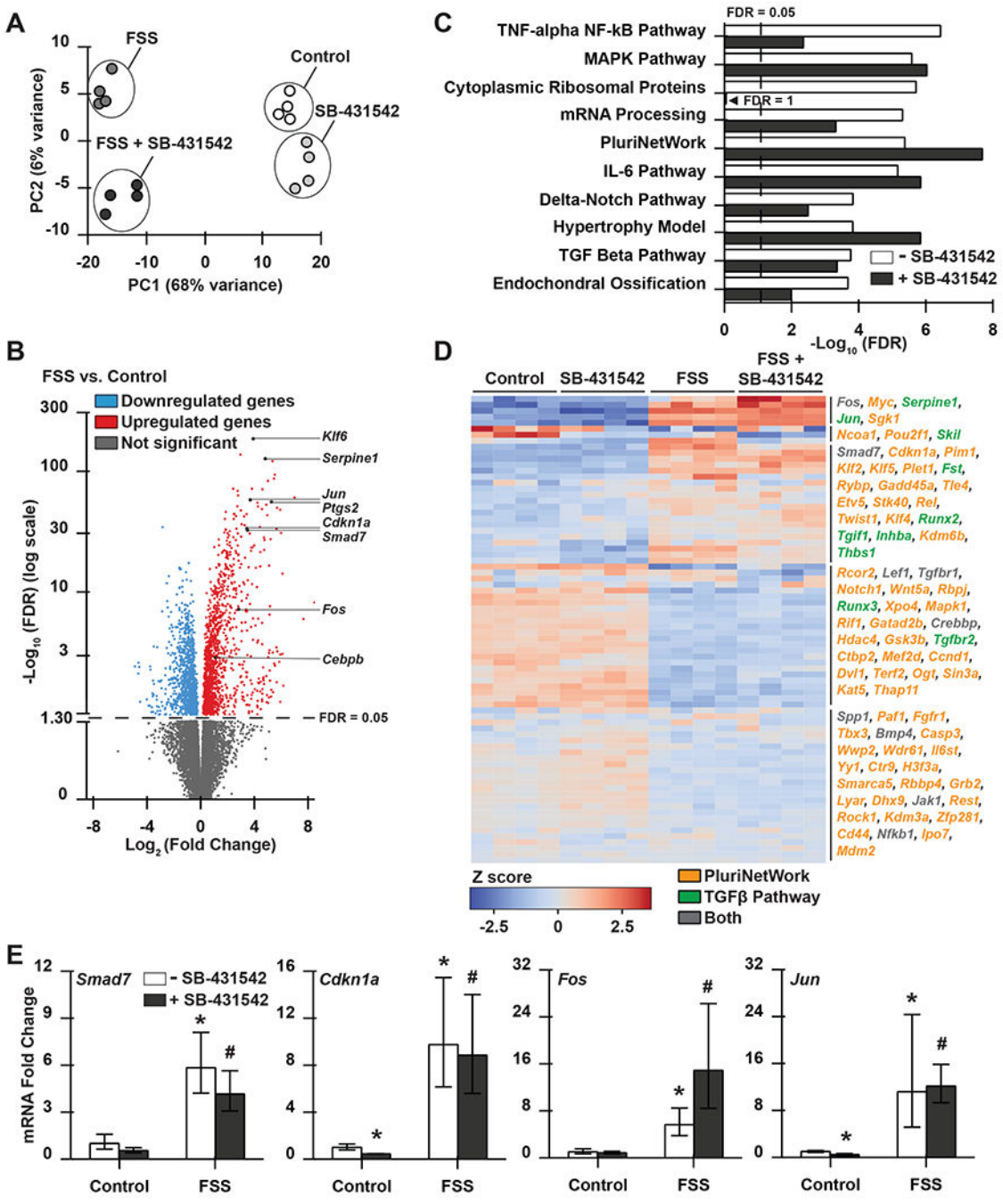

Figure 6: RNAseq analysis supports potent FSS regulation of TGFβ superfamily signaling.

(A) Principal component analysis of sample variation considering the 500 genes with greatest variance. (B) Volcano plot showing the distribution of differential gene expression in FSS-stimulated and unstimulated cells, and identifying induced (red) and repressed (blue) differentially expressed genes (DEGs). (C) Enrichr pathway analysis using the WikiPathways database reveals the top ten most significantly regulated pathways, including TGFβ, that remain significantly regulated even in the presence of SB-431542. (D) Genes related to the TGFβ and PluriNetWork pathways were clustered in a heatmap, and genes in

each cluster are grouped. (E) qRT-PCR analysis of established TGFβ-inducible genes *Smad7*, *Cdkn1a*, *Fos*, and *Jun* following FSS stimulation in the presence or absence of SB-431542. Vehicle is 1% DMSO. Dotted lines on graphs indicate threshold for statistical significance (FDR<0.05). *p<0.05 compared to unstimulated cells and #p<0.05 compared to SB-treated controls.

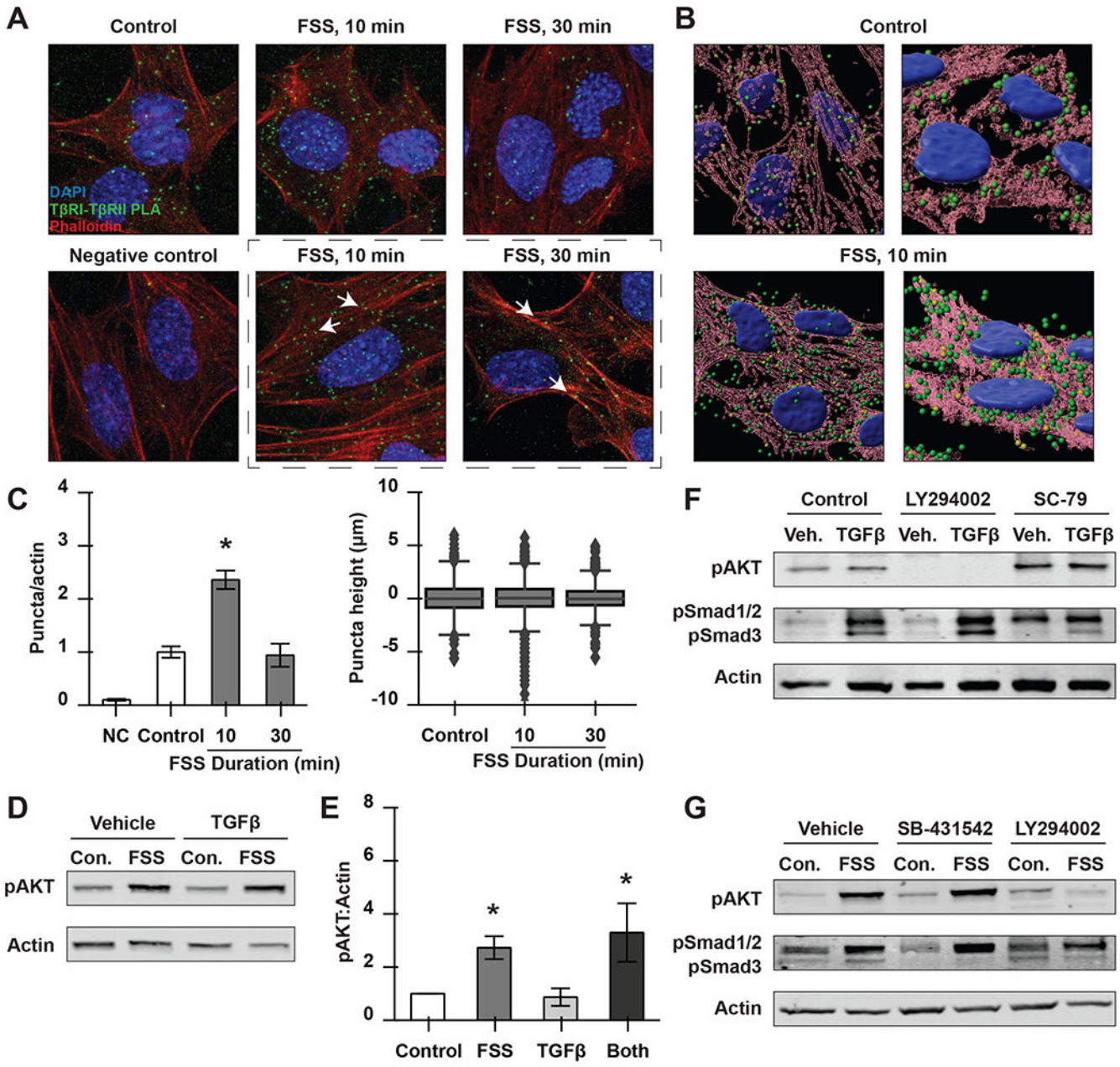

Figure 7: FSS-dependent regulation of TGFβ receptor heteromerization.

(A) Images of proximity ligation assay (PLA) between TβRI and TβRII (n=5 regions of interest). Dashed lines show puncta localization relative to Actin fibers. (B, C) IMARIS analysis of images (B) allows quantitative analysis of puncta frequency and spatial distribution in the presence or absence of FSS (C). (D, E) Western analysis and quantification of control cells and cells treated with TGFβ or stimulated with FSS (30 minutes). (F) Representative western analysis from cells pretreated (60 minutes) with vehicle or a PI3K/AKT inhibitor (LY294002) or agonist (SC-79) followed by treatment with TGFβ (30 minutes). (G) Representative western analysis from cells pretreated (60 minutes)

with vehicle or a TβRI or PI3K/AKT inhibitor followed by treatment (30 minutes) with 0.1 Pa FSS. All values normalized to control cells. *p<0.05 compared to unstimulated cells.

Table 1:

TaqMan probe IDs for qRT-PCR

Gene	TaqMan probe ID
Rn18s	Mm03928990_g1
Ptgs2	Mm00478374_m1
Serpine1	Mm00435858_m1
Smad7	Mm00484742_m1
Cdkn1a	Mm04207341_m1
Fos	Mm00487425_m1
Jun	Mm00495062_s1